Journal of Microscopy, Vol. 210, Pt 3 June 2003, pp. 262–268
Received 10 August 2002; accepted 25 October 2002

A versatile multipurpose scanning probe microscope

E. CEFALÌ*, S. PATANÈ*, P. G. GUCCIARDI†, M. LABARDI‡ & M. ALLEGRINI‡

* *INFM and Dipartimento di Fisica della Materia e Tecnologie Fisiche Avanzate, Università di Messina, Salita Sperone 31, I-98166 Messina, Italy*

†*CNR, Istituto per i Processi Chimico Fisici, Sez. di Messina, Via La Farina 237, I-98123 Messina, Italy*

‡*INFM and Dipartimento di Fisica, Università di Pisa, Via Buonarroti 2, I-56127 Pisa, Italy*

Key words. Atomic force microscopy, scanning near-field optical microscopy, scanning probe microscopy, scanning tunnelling microscopy.

Summary

A combined scanning probe microscope has been developed that allows simultaneous operation as a non-contact/tapping mode atomic force microscope, a scattering near-field optical microscope, and a scanning tunnelling microscope on conductive samples. The instrument is based on a commercial optical microscope. It operates with etched tungsten tips and exploits a tuning fork detection system for tip/sample distance control. The system has been tested on a *p*-doped silicon substrate with aluminium depositions, being able to discriminate the two materials by the electrical and optical images with a lateral resolution of 130 nm.

Introduction

Combined scanning probe microscopes (SPMs) attract particular interest in materials and surface science since they are able to provide correlation on the local scale among the simultaneously measured quantities, electrical, mechanical or optical.

Among the numerous combinations reported in the literature are SNOM/STM (Pohl *et al.*, 1984; Nakajima *et al.*, 1999), SNOM/AFM (Zenhausern *et al.*, 1994; Orlik *et al.*, 2000), and AFM/STM (Murrell *et al.*, 1993). Typically, the AFM section operates in contact (Houze *et al.*, 1996) and in non-contact mode (Garcia *et al.*, 1999). It has also been shown that it is possible to acquire the tunnelling current in the tapping mode (Sarid, 1996; Fein *et al.*, 2001) or more generally in the dynamic mode (Loppacher *et al.*, 2000).

Generally, these instruments are operated using either the current or the force to stabilize the tip–sample distance (constant gap mode, CGM) to a value in the nanometre range that ensures the near-field condition for the optical interaction. Therefore, a 'topographic' map is obtained that corresponds rather to a surface of constant current or force. The near-field optical signal is not suitable for this purpose, since its distance dependence is not as steep as for the other cases, and also because of the higher background level. Although the stabilization may introduce topographic (or *z*-motion) artefacts (Hecht *et al.*, 1997), it remains the best way to ensure the near-field condition, both removing long-time drifts and avoiding tip damages. The issue of topographic artefacts in scanning probe microscopy, and especially in SNOM, is well known; from a phenomenological point of view, artefacts originate from the correlation between the topography signal (driven by a servo-loop) and the other measured quantities (in our case the optical and the electrical signals). Constant-height mode operation does not yield such problems, but it is rarely used owing to experimental complications. A scanning probe microscope able to provide three different surface properties, one of which is used for distance stabilization (and thus is stabilized by the feedback loop to a constant value), deserves special attention. The additional two quantities are not restricted to a single value, but on the contrary they are free to assume a range of values, allowing correlation studies.

In this paper, we report on the realization of a tapping-mode atomic force microscope with simultaneous measurement of the tunnelling current and of the scattered optical signal (AFM/STM/SNOM). We also introduce a 2D histogram technique correlating the maps of the different acquired physical quantities, which permits us to draw quantitative conclusions about the occurrence of topography artefacts. In practice, with our set-up we have acquired and compared topography with optical images as well as with electrical images, their correlation being deduced through the 2D histogram technique. In the Materials and methods section, the experimental setup will be described with special emphasis on the tip choice and on its method of production. Preparation of a special sample for testing the simultaneous measurement capability of the

Correspondence: Dr S. Patane. E-mail: salvatore.patane@unime.it

instrument is also described. We then show the simultaneous images of topography, current and optical scattering on the test sample, also analysed by a 2D histogram technique used for image correlation.

Materials and methods

Experimental set-up

The instrument is represented in Fig. 1. The probe microscope head has been adapted to a commercial optical microscope (Zeiss Axiotech Vario) and it is depicted in the inset to Fig. 1. Basically, the tip can be translated in order to be placed in the focus of the long-working-distance objective of the optical microscope. The scanning stage holding the sample can be moved by an XYZ micrometre stage. The use of the frame of an optical microscope facilitates the placement of the tip in correspondence to the illumination laser spot for SNOM operation, as well as the location of the desired sample area. The whole set-up rests on top of a vibration-damping stage. The head is interfaced to a commercial SPM control unit (SCALA, Omicron GmbH) based on a SUN Sparc Workstation.

AFM operation is accomplished in the non-contact or tapping mode, depending on the chosen vibration amplitude of the tip. The force detection is made by a quartz tuning fork (Karrai & Grober, 1995) mounted with the prongs parallel to the sample surface; the tip, bent at the edge, is glued to one arm of the fork that is dithered by means of a piezo slab (see inset to Fig. 1) and oscillates at the fork-tip assembly resonance ($f_0 = 32768$ Hz). The attachment of the tip causes a shift of the free fork resonance by $\Delta f \approx -500$ Hz. The typical Q-factor is 1100 and the tuning fork stiffness is about 26 500 N m^{-1}. Such parameters are well suited for tapping mode operation (Rensen *et al.*, 1999). The fork resonance is excited by means of a function generator and the resulting oscillation amplitude, measured by lock-in techniques, is stabilized to a set value by the distance control feedback loop that adjusts the sample z position. The calibration of the

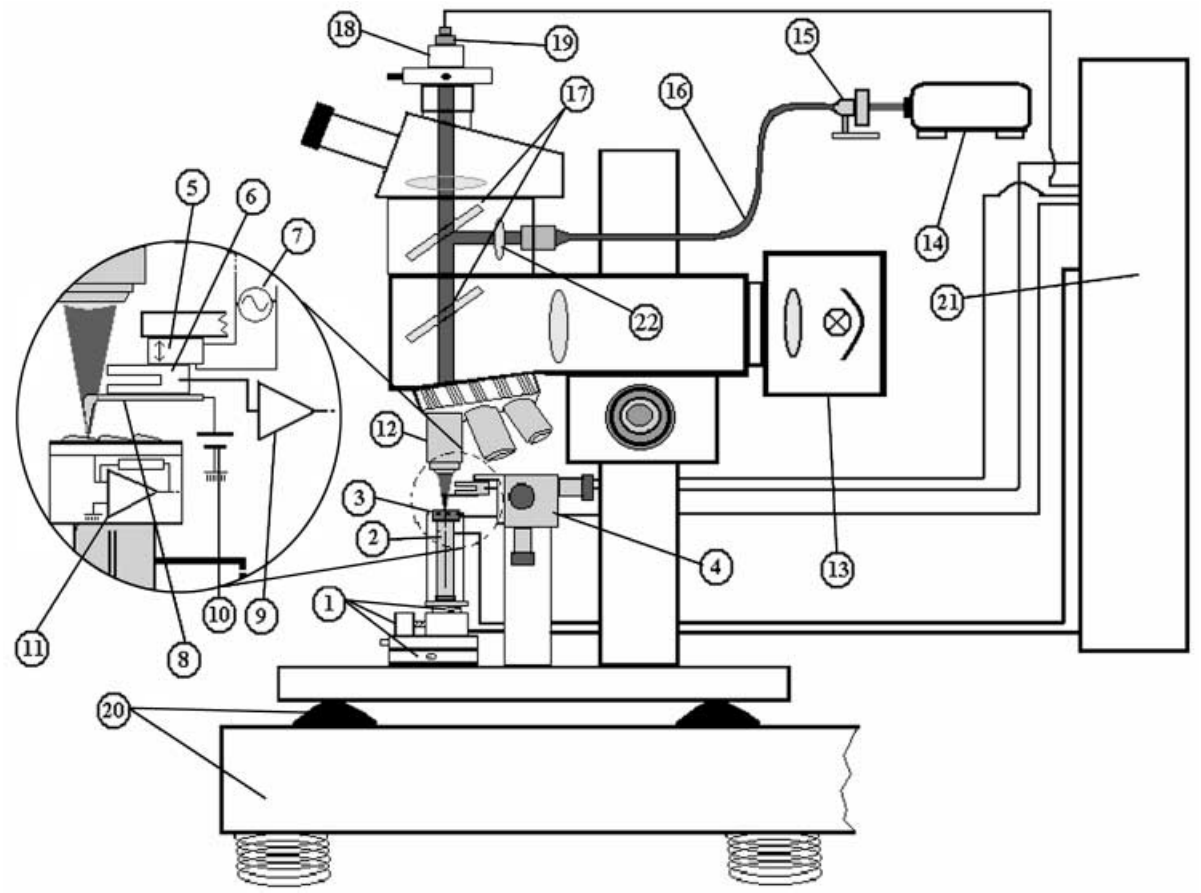

Fig. 1. Schematic of the combined SPM. Legend: (1) XYZ coarse motion stage, (2) piezo tube, (3) sample holder, (4) XYZ micrometre translation stage, (5) dithering piezo slab, (6) quartz tuning fork, (7) function synthesizer, (8) metallic tip, (9) tuning fork signal preamplifier, (10) voltage bias supply, (11) I/V preamplifier, (12) microscope objective, (13) lamp, (14) laser diode, (15) optical fibre coupler, (16) single-mode optical fibre, (17) beam splitter, (18) filters, (19) photodiode, (20) damping base and isolated optical table, (21) control system (lock-in, SPM controller, SUN workstation), (22) lens.

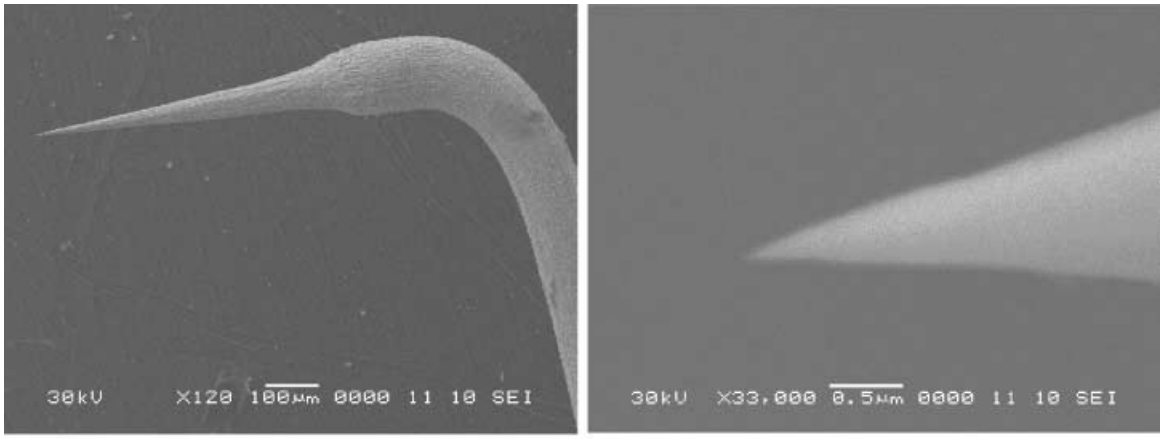

Fig. 2. SEM micrographs of a tungsten metallic probe: (a) overview; (b) high-resolution zoom on the tip.

fork oscillation amplitude can be performed by means of an adaptable interferometric set-up (Toledo-Crow *et al.*, 1992) not shown in the figure.

For electrical conductivity measurements, the tip–sample junction is biased and the current detected by a low-noise current preamplifier mounted inside the scanning stage. The current signal, modulated at the tip vibration frequency, is conveniently detected by lock-in techniques as well.

The SNOM section is realized as follows. The light from a 645-nm laser diode is coupled into a single-mode fibre whose output is collimated by a lens and focused on the tip apex by means of a 50× microscope objective (NA 0.55), after being reflected at 90° by a beam splitter. The same objective is used to collect the scattered light that is subsequently detected by a photodiode. The optical signal is thus demodulated by another lock-in amplifier referenced to the tapping-mode frequency.

The probes

The key element in obtaining high performance in such a combined microscope is the probe. The requirements are: (i) a suitable shape and stiffness for AFM tapping mode operation; (ii) light scattering efficiency for SNOM operation and (iii) good electrical conductivity for STM operation. Tungsten satisfies all these requirements. It is traditionally used to build STM tips (Cricenti *et al.*, 1994) and is also a good light scatterer for SNOM purposes (Bachelot *et al.*, 1997).

Our probes are obtained by electrochemical etching of a 100-µm tungsten wire, following standard recipes for STM tips (Melmed, 1991) able to produce tips of apical radius ranging from 10 nm to 100 nm with a remarkable degree of reproducibility. Furthermore, to reduce the optical signal background arising from the reflection of the tuning fork arms, we have optimized the horizontal and vertical cantilever length and its geometry, taking into account the NA of the objective and its working distance. SEM micrographs of a tungsten probe are shown in Fig. 2.

The sample

The sample used for the test measurements is a nanostructured pattern of Al deposited on a *p*-doped Si substrate. It is obtained with standard techniques: a layer of latex spheres (diameter 1000 nm) is deposited by means of dip coating on a substrate previously etched in a bath of HF to eliminate the native oxide surface layer. Subsequently, the sample is thermally evaporated with a 20-nm-thick Al film. Finally, the latex spheres are removed by an ultrasonic ethanol bath. The result is a sample with low topography (average height 20 nm) showing high optical and electrical contrast between the Al islands and the Si substrate.

Results and discussion

In Fig. 3 we can see the simultaneous topographic (a), electrical (b) and optical (c) images of the Al/p-Si test pattern. The topographic image shows a variety of different Al patterns with various shapes and the expected flat topography, the average height being about 25 nm and the maximum height 40 nm. The Al islands show a higher optical signal than the silicon substrate, with a mean optical contrast of about 34%. They also show higher conductivity than the substrate. The range of measured currents (µA) is in agreement with data reported in the literature (Fein *et al.*, 2001). Arrows on Fig. 3(b) indicate points where the current signal is not correlated with topographic features. Such local variations of the conductivity could be ascribed to impurities or to aluminium oxide formation. The optical image shows zones where the Al islands have higher reflectivity, but no correlation with both topography and electrical signal is revealed (solid arrows in

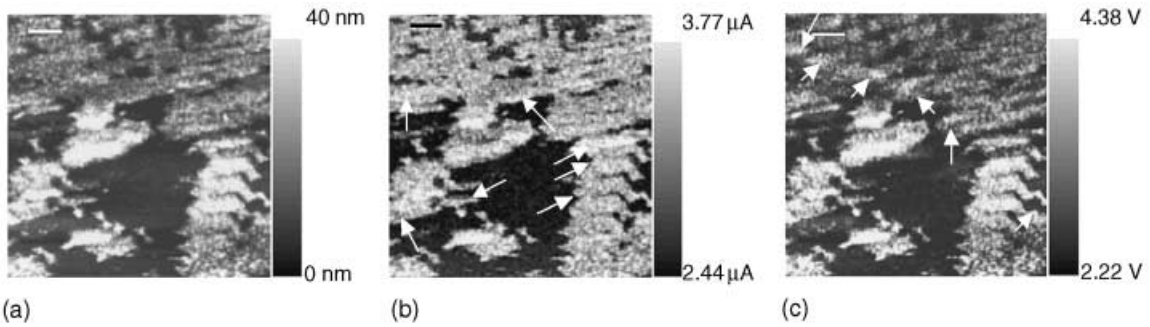

Fig. 3. Topography (a), electrical current (b) and optical signal (c) images on a sample of Al pattern on Si *p*-doped substrate. The images have been acquired simultaneously. Scan area: 10 μm × 10 μm; scale bar: 1 μm. On the optical image, solid arrows indicate zones with higher reflectivity not correlated with the topography and with the current images. On the electrical current image, zones with higher (solid arrows) and lower (dotted arrows) conductivity not correlated with the topography are indicated.

Fig. 3c). To study the image correlation on a statistical basis we have applied a 2D-histogram technique, as reported in the AFM literature (Luthi *et al.*, 1995; Carpick & Salmeron, 1997), and which is useful for the study of the friction force dependence as a function of the load. The technique consists of plotting a histogram $N(A,B)$ where $A(x,y)$ and $B(x,y)$ are the measured quantities, x and y being the coordinates of the image, and N the frequency of the particular pair of values A and B. In the case of high correlation, the plot shows grouping of the histogram points. Low correlation translates to wider spreading of the points.

Figure 4(a) shows the 2D histogram correlating the topography and current images of Fig. 3. We notice a region of the histogram corresponding to low topography and lower conductivity (bottom left), a region with topography between 15 and 35 nm with a rather narrow interval of conductivity, and a third region ranging from 20 to 35 nm and higher values of conductivity, but spread on a wider range. Thus, the electrical behaviour of the different materials is easily identified by this type of plot.

Figure 4(b) shows the 2D histogram concerning the topography vs. SNOM optical signal images of Fig. 3. The plot shows that the points are grouped around the diagonal, indicating an average proportional trend of the two signals. Furthermore, a remarkable spread of the data around the main trend is visible. Such a spread indicates that there are zones of the Al islands with a local variation of the reflectivity. The optical signal dependence vs. topography can be ascribed to *z*-motion artefacts, since the measured value (about 1.6% nm^{-1}) is consistent with the usual values recorded in aperture-SNOM setups (Hecht *et al.*, 1997). Nevertheless, an artefact effect would produce much higher grouping of the histogram points around the diagonal. Furthermore, the artefact contribution could have the opposite trend as well (contrast inversion) (Gucciardi & Colocci, 2001). Assessing the presence of artefacts would require further investigation.

On the other hand, the effect of the optical properties of the thin metal film (Heavens, 1991) on the optical images can be

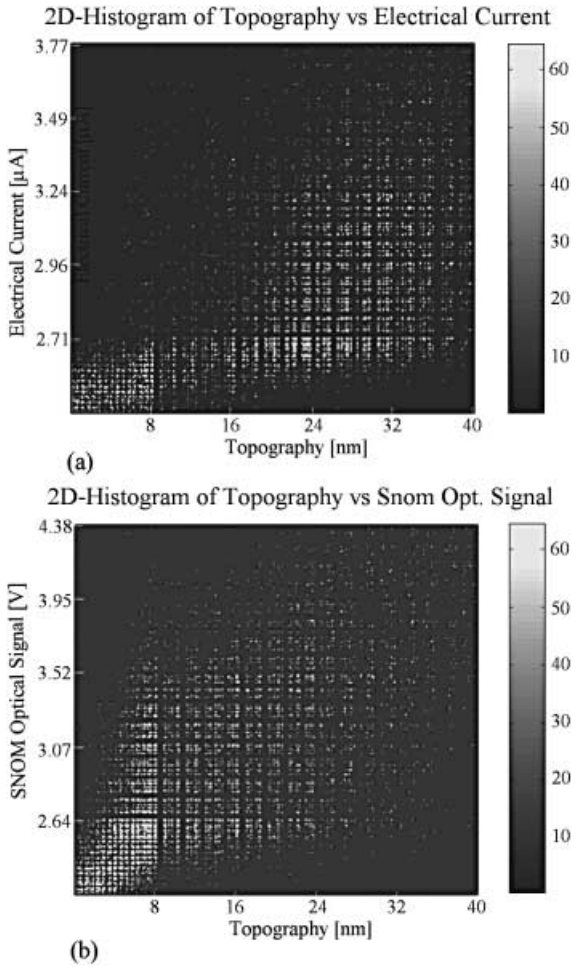

Fig. 4. 2D histograms correlating the images in Fig. 3: (a) topography vs. electrical current; (b) topography vs. SNOM optical signal.

estimated. Figure 5 shows the far-field reflectivity of an Al thin film on an Si substrate as a function of film thickness. The near-field decay length is comparable to the tip diameter of about 100 nm. Therefore, we assume the optical properties

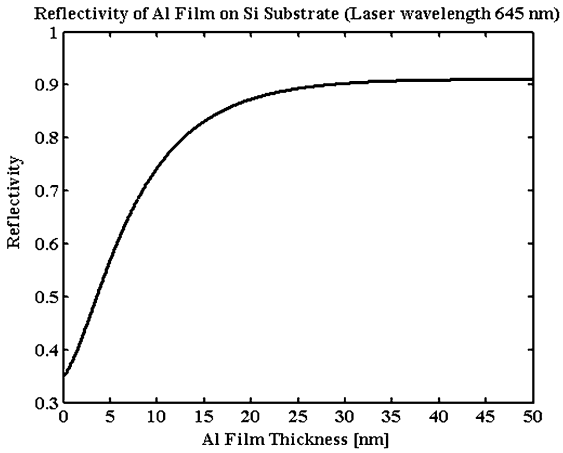

Fig. 5. Calculated far-field reflectivity of an Al film on an Si substrate as a function of the film thickness.

of the film as if they were concerned by propagating light, as far as the film thickness does not overcome the decay length. Under such an approximate assumption, we observe that the reflectivity increases up to 30 nm thickness. The sign of the expected contrast is thus consistent with the experimental result (brighter for thicker film). The optical image is consistent with the optical properties of the sample, even if the influence of *z*-motion artefacts cannot be excluded.

Another set of images, acquired on a smaller area and applying a bias voltage of 1 V, is shown in Fig. 6 (a: topography, b: electric current, c: optical signal). Both the optical (mean optical contrast of about 53%) and the electrical current images display zones where the signal is not correlated with the topography (these zones are marked by arrows). To evaluate the resultant resolution we have extracted the profiles along the marked line on the images and applied the Rayleigh-type criterion. The resolution is about 130 nm, which is consistent with the tip diameter used. A comparison of the three profiles extracted at the same position shows that the optical profile is laterally shifted about 50 nm with respect to both the electrical and the topographic profile. Such a shift could be due to the fact that the optical scattering centre does not match with the apical centre responsible for the electrical tunnelling and the mechanical interaction. Further experiments with smaller tip radii and using higher harmonic lock-in detection for suppression of topographic artefacts (Labardi *et al.*, 2000; Maghelli *et al.*, 2001) are in progress.

Conclusions

The instrument we have realized is characterized by a high degree of versatility and could be fruitfully applied to investigate on the nanometre scale several systems of interest in materials and surface science. Potential resolution on the nanometre scale even for the optical section is expected, since scattering-type near-field optical microscopy has recently undergone remarkable improvements, especially when using metal tips. In order to check the potential of this microscope, imaging of a suitable home-made sample have been carried out, achieving an ultimate lateral resolution of about 130 nm. Image analysis has been carried out using the 2D histogram technique to check and discriminate pure signal from possible artefacts. No significant topographic artefacts were present, suggesting that the instrument is able to provide simultaneous information about the topography, the electrical conductivity and the optical properties of the sample. The experimental as well as the post-processing techniques applied here are promising for the study of the correlation of quantities of different nature measured on nanoscale systems.

Acknowledgement

We are grateful to INFM-MURST for the financial support through the project 'SUD-NanoSNOM'.

References

Bachelot, R., Gleyzes, P. & Boccara, A.C. (1997) Reflection-mode scanning near field optical microscopy using an apertureless metallic tip. *Appl. Opt*. **36**, 2160–2170.

Carpick, R.W. & Salmeron, M. (1997) Scratching the surface: fundamental investigations of tribology with atomic force microscopy. *Chem. Rev*. **97**, 1163–1194.

Cricenti, A., Paparazzo, E., Scarselli, M.A., Moretto, L. & Selci, S. (1994) Preparation and characterization of tungsten tips for scanning tunneling microscopy. *Rev. Sci. Instrum*. **65**, 1558–1560.

Fein, A., Zhao, Y., Peterson, A., Jabbour, G.E. & Sarid, D. (2001) Individually injected current pulses with conducting-tip, tapping-mode atomic force microscopy. *Appl. Phys. Lett*. **79**, 3935–3937.

Garcia, R., Calleja, M. & Rohrer, H. (1999) Patterning of silicon surfaces with non contact atomic force microscopy: field induced formation of nanometer-size water bridges. *J. Appl. Phys*. **86**, 1898–2003.

Gucciardi, P.G. & Colocci, M. (2001) Different contrast mechanisms induced by topography artifacts in near-field optical microscopy. *Appl. Phys. Lett*. **79**, 1543–1545.

Heavens, O.S. (1991) *Optical Properties of Thin Solid Films*. Dover Publishers, New York.

Hecht, B., Bielefeldt, H., Inouye, Y., Pohl, D.W. & Novotny, L. (1997) Facts and artifacts in near-field optical microscopy. *J. Appl. Phys*. **81**, 2492–2498.

Houze, F., Meyer, R., Schneegans, O. & Boyer, L. (1996) Imaging the local electrical properties of metal surfaces by atomic force microscopy with conducting probes. *Appl. Phys. Lett*. **69**, 1975–1977.

Karrai, K. & Grober, R.D. (1995) Piezoelectric tip-sample distance control for near field optical microscopes. *Appl. Phys. Lett*. **66**, 1842–1844.

Labardi, M., Patanè, S. & Allegrini, M. (2000) Artifact-free near-field optical imaging by apertureless microscopy. *Appl. Phys. Lett*. **77**, 621–623.

Loppacher, Ch, Bammerlin, M., Guggisberg, M., Schaer, S., Bennewitz, R., Baratoff, A., Meyer, E. & Guntherodt, H.J. (2000) Dynamic force

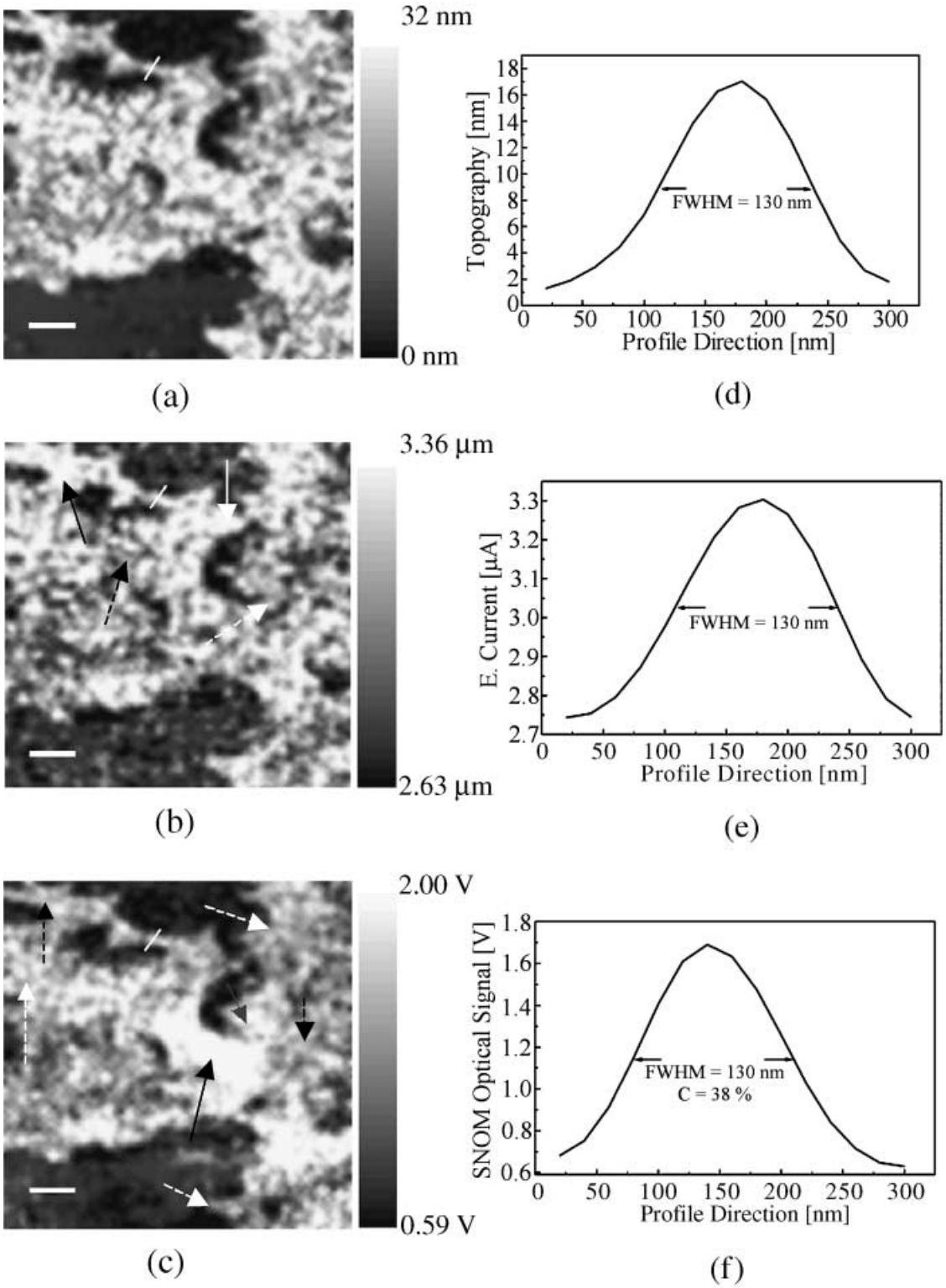

Fig. 6. (a) Topography, (b) electrical and (c) optical images acquired on a smaller area (4 µm × 4 µm). Scale bar: 500 nm. On the optical image, zones with higher (solid arrows), and lower (dotted arrows) reflectivity not correlated with the topography are shown. On the electrical current image, zones with higher (solid arrows) and lower (dotted arrows) conductivity not correlated with the topography are marked. (d–f) Profiles extracted along the white line on images (a–c), respectively.

microscopy of copper surfaces: atomic resolution and distance dependence of tip–sample interaction and tunnelling current. *Phys. Rev. B*, **62**, 16944–16949.

Luthi, R., Meyer, E., Haefke, H., Howald, L., Gutmannesbauer, W., Guggisberg, M., Bammerlin, M. & Guntherodt, H.J. (1995) Nanotribology: An UHV-SFM study on thin films of C_{60} and AgBr. *Surf. Sci.* **338**, 247–260.

Maghelli, N., Labardi, M., Patanè, S., Irrera, F. & Allegrini, M. (2001) Optical near-field harmonic demodulation in apertureless microscopy. *J. Microsc.* **202**, 84–93.

Melmed, A.J. (1991) The art and science and other aspects of making sharp tips. *J. Vac. Sci. Technol. B*. **9**, 601–608.

Murrell, M.P., Welland, S.J., Oshea, T.M., Wong, J.R., Barnes, R., McKinnon, A.W., Heyns, M. & Verhaverbeke, S. (1993) Spatially resolved electrical measurements of SiO_2 gate oxide using atomic force microscopy. *Appl. Phys. Lett*. **62**, 786–788.

Nakajima, K., Micheletto, R., Mitsui, K., Isoshima, T., Hara, M., Wada, T., Sasabe, H. & Knoll, W. (1999) Nanoscopic studies investigated by hybrid SNOM/STM. *Appl. Surf. Sci*. **144**, 520–524.

Orlik, X.K., Labardi, M. & Allegrini, M. (2000) Nanometer scale observation of ferroelectric domains using an apertureless near field optical microscope. *Appl. Phys. Lett*. **77**, 2042–2044.

Pohl, D.W., Denk, W. & Lanz, M. (1984) Optical sthetoscopy image recording with resolution $\lambda/20$. *Appl. Phys. Lett*. **44**, 651–653.

Rensen, W.H.J., van Hulst, N.F. & Ruiter & West, P.E. (1999) Atomic steps with tuning fork-based non contact atomic force microscopy. *Appl. Phys. Lett*. **75**, 1640–1643.

Sarid, D. (1996) Tapping mode scanning force microscopy: Metallic tip and samples. *Comput Mater. Sci*. **5**, 291–297.

Toledo-Crow, R., Yang, P.C., Chen, Y. & Vaez-Iravani, M. (1992) Near field differential scanning optical microscope with atomic force regulation. *Appl. Phys. Lett*. **60**, 2957–2959.

Zenhausern, F., O'Boyle, M.P. & Wickramasinghe, H.K. (1994) Apertureless near-field optical microscope. *Appl. Phys. Lett*. **65**, 1623–1625.